Solving the Helmholtz Equation for Exterior Problems with Variable Index of Refraction. I,

by

Gregory A. Kriegsmann

Department of Mathematics and Statistics

University of Nebraska-Lincoln

Lincoln, Nebraska 68588

Cathleen S. Morawetz

Courant Institute of Mathematical Sciences,

New York University

251 Mercer Street

New York, New York 10012

Dedicated to R.D. Richtmeyer
on the occasion of his 70th birthday

Results obtained at the Courant Institute of Mathematical Sciences, New York University, with AFSOR, Contract, F49620-79-C-0193, and Contract N00014-76-C-0439.

ABSTRACT

A new technique for numerically solving the reduced wave equation on exterior domains is presented. The method is basically a relaxation scheme which exploits the limiting amplitude principle. A modified boundary condition at "infinity" is also given. The technique is tested on several model problems: the scattering of a plane wave off a metal cylinder, a metal strip, a Helmholtz resonator, an inhomogeneous cylinder (lens), and a nonlinear plasma column. The results are in good qualitative agreement with previously calculated values. In particular, the numerical solutions exhibit the correct refractive and diffractive effects at moderate frequencies.

1. Introduction

It is well known that for dissipative linear ordinary differential equations with a forcing term of period λ that the transients die out and the solution tends as $t \to \infty$ to solutions of period λ. The same is true of many hyperbolic equations. In particular solutions of the wave equation in infinite domains with appropriate boundary conditions and with the forcing term $fe^{i\omega t}$ tend, for large times, to solutions of the Helmholtz equation $\Delta u + \omega^2 u = f$. This is known as the limiting amplitude principle [10].

The purpose of this paper is to show that a varied form of a limiting amplitude principle can be used to solve numerically, in a short time and for a rather wide variety of geometries, the Helmholtz equation in the exterior of an obstacle with a variable index of refraction. Furthermore this can be done at such high frequencies that a great deal of geometric optical behavior can be confirmed even on a relatively coarse mesh.

The Helmholtz equation with variable index of refraction is

$$\Delta u + \omega^2 n u = 0$$

where the index of refraction $n = n(\vec{x})$ is a function of the space variables $(\vec{x})$. We also consider situations where $n = n(\vec{x}, |u|)$ which corresponds to certain models of laser beam propagation. At large distances we assume $n \to$ constant which may be scaled to 1. Then the parameter ω has the dimension of $[\text{Length}]^{-1}$ and the appropriate dimensionless constant is ωa where a is a characteristic length of the scatterer. It may range from zero to infinity.

The field u is given as a plane wave $e^{i\omega x}$ and its scattered field u_s;

$$u = e^{i\omega x} + u_s. \tag{1.1}$$

However, the source could equally well be located at a finite

point in the plane. The scattered field satisfies the outward radiation condition

$$\frac{\partial u_s}{\partial r} - i\omega u_s + \frac{u_s}{2r} \to 0 \tag{1.2}$$

as $|x| \to \infty$.

This problem may be studied using geometrical optics for high frequency and expansion in ω for low frequency. Our original objective was to deal with the range of frequency where neither of these approximations is good. We found, in addition, however, that many of the features of geometrical optics emerge from the computations at moderate frequencies. Primarily though, we are concerned with perturbations in the index of refraction or with disturbing objects where the characteristic length is not large compared to the wave length.

A wave at frequency ω has the wave length $2\pi/\omega$ and theoretically for geometrical optics one needs $2\pi/\omega << a$. Our observations confirm that in many applications $\omega a = 5$ or 10 displays the significant features of geometrical optics and diffraction theory.

In this paper we restrict ourselves to two dimensional examples. In a second paper we plan to demonstrate results in axi-symmetric and possibly three dimensional geometries. A particular advantage in 2D is that every simply-connected object can be studied by noting that it can be mapped conformally onto the exterior of a circle and the transformation

induces a new Helmholtz equation for the solution with a new index of refraction. In fact, however, we have also computed objects that are not simply-connected but have rectangular boundaries in polar coordinates.

The principal results of interest are:

(i) Confirmation of the scattering cross section for a cylinder of radius one with a Dirichlet boundary condition. Results are compared with those presented by Bowman, Senior, and Uslenghi [1]. The error is less than 1(10) % at the frequency ω = 5 (10) . The computations also show that the position of the shadow edge, as given by geometrical optics, is within one or two mesh points.

(ii) The diffraction by an infinite strip of half-width 2 at various angles to an incident plane wave. There is good correlation with [1] particularly at low frequencies and at an angle of 45° and with geometrical optics [1].

(iii) The computations of the field including the cross-section of a Helmholtz resonator of radius 1 with various apertures and for plane waves at various angles of incidence.

(iv) The refraction of a plane wave by a lens of either constant or variable index of refraction.

In particular we include lenses that produce focusing and caustics such as the Luneberg lens.

(v) The refraction by a model of an overdense plasma.

The method of computation is a modification of the relaxation method used in [2] and is described in Section 2. To reduce the number of mesh points involved a modified radiation condition corresponding to (2) is imposed at a finite radius (see Section 3). The difference scheme and how to deal with the artificial singularity at the origin created by using polar coordinates is described in Section 4. In Section 5, we describe in detail the particular examples computed. In each case we give the running times on the CDC 6600 required to achieve convergence. The effects of applying the modified radiation condition at different distances are also discussed.

In Section 6 we discuss the limitations of this kind of iterative method and other possible applications.

The authors are grateful to F. Tappert for much advice and many suggestions. The work of A. Bayliss and E. Turkel [3] on similar problems with obstacles treats the radiation condition using the same ideas. Turkel pointed out to the

authors that the modified radiation condition is well posed in the sense of Kreiss-Lobatchinskii [11].

2. The Iteration Method.

We consider a time dependent equation

$$(Q\tilde{U})_t = \Delta\tilde{U} + n\omega^2\tilde{U} \tag{2.1}$$

where Q is a first order operator in the space variables, $Q = 2\vec{a}\cdot\nabla + b$. The coefficient vector $\vec{a}$ and the scalar b are chosen so that the solutions of (2.1) of the form plane wave or source plus outgoing scattered wave will approach a time independent state. This will be the desired solution.

This method was used in [2]. However, (2.1) was used directly, i.e. in characteristic form. Data was given on a characteristic surface. The convergence was therefore very slow because a very small time step was required for stability with the space differences used.

In the present method we transform (2.1) to a Cauchy problem by a change of variables given by

$$\begin{aligned} dt' &= dt + \vec{a}\cdot d\vec{x} \\ d\vec{x}' &= d\vec{x}. \end{aligned} \tag{2.2}$$

We obtain in the new variables

$$|\vec{a}|^2\tilde{U}_{tt} = \Delta\tilde{U} + \tilde{U}_t(\nabla\cdot\vec{a} - b) + n\omega^2\tilde{U} \tag{2.3}$$

where we have dropped the primes. We now solve an initial value problem which by our choice of $\vec{a}$ and b will converge to the steady state. For example, the convergence has been

improved by more than an order of magnitude in the case

$$\vec{a} = \vec{x}/|\vec{x}|, \quad b = -2i\omega + \nabla\cdot\vec{a}. \tag{2.4}$$

In two dimensions with $\vec{a}$, b given by (2.4) we introduce in (2.3) the change of variable:

$$\tilde{U} = e^{i\omega x} + \frac{\tilde{W}e^{i\omega t}}{\sqrt{r}} \tag{2.5}$$

with $|\vec{x}| = r$. Equation (2.3) reduces in polar coordinates to

$$\tilde{W}_{tt} = \tilde{W}_{rr} + r^{-2}[\tilde{W}_{\theta\theta} + \tfrac{1}{4}\tilde{W}] + \omega^2(n-1)\tilde{W} + \omega^2\sqrt{r}(n-1)e^{i\omega(x-t)} \tag{2.6}$$

which for n = 1 is the wave equation. However, in general it has fixed characteristics that are independent of n. Thus if n = 1 we are using the standard limiting amplitude principle but since in some of our examples n changes dramatically it is a great advantage that the characteristics are fixed. For $n \neq 1$ we are solving a wave equation with potential.

From [2] we have the growth restriction to obtain decay

$$\frac{\partial}{\partial r}[r(n-1)] > 0. \tag{2.7}$$

If this condition is not satisfied we are dealing with a potential which has bound states that give rise to exponentially growing solutions of (2.6). This showed up numerically in a very dramatic fashion when we tried lenses with n > 1. The inequality (2.7) was proved by J. Weidmann [4] as a necessary condition to prevent these growing modes.

In order to handle this situation we note that instead of (2.6) we could use

$$(2.8)\qquad n_1\tilde{W}_{tt} = \tilde{W}_{rr} + r^{-2}[\tilde{W}_{\theta\theta}+\tfrac{1}{4}\tilde{W}] + (n_2-1)\omega^2\tilde{W} + \omega^2\sqrt{r}(n-1)e^{i\omega(x-t)}$$

where $n_1 + n_2 = n + 1$. If the limiting amplitude principle holds, i.e. the potential $(n_2-1)\omega^2$ does not give rise to growing modes and $n_1 > 0$, then the solutions of (2.8) also approach a time harmonic steady state and the space dependent coefficient satisfies the desired Helmholtz equation.

If we make $n_1 > 1$ in such a way that $[r(n_2-1)]_r \geq 0$, then (2.8) can be used for the iteration. We have applied this notion only for $n_1 = n \geq 1$, $n_2 = 1$ and $n \leq 4$ inside a circle. Note that the Courant-Friedrichs-Lewy condition for the time step continues to be satisfied over $n_1 > 1$ if it holds for $n_1 = 1$. On the other hand if there are trapped rays produced by the artificial index n_1 then the approach to steady state may be exceedingly slow as the higher frequencies have poorer exponential decay.

3. Improving the Radiation Condition and Finding the Scattering Cross Section.

Returning to the original radiation condition (1.2) we note that if a solution satisfies the radiation condition, then by using the fundamental solution representation for the reduced wave equation, we have with $u_s = Wr^{-(N-1)/2}e^{i\omega r}$ the expansion

$$W = \sum_{j=0}^{\infty} A_j r^{-j} \tag{3.1}$$

in any number of dimensions. Here A_j is a function of ω and the angular variables. The differential equation for W at large distances is

$$2iW_r = -W_{rr} - \frac{1}{r^2} LW \tag{3.2}$$

where L is a differential operator acting on the angular variables (the Laplace-Beltrami operator). We have rescaled r so that $\omega = 1$. On substituting the expansion for W we find the recursion formula

$$A_{n+1} = \tilde{P}(n+1,L)A_n, \quad n \geq 0 \tag{3.3}$$

where $\tilde{P}(n+1,L) = -\frac{1}{2}i\ (n+1)^{-1}\ \{L+n(n+1)\}$. Note that $\tilde{P}(1,L) = -\frac{i}{2} L$. Next we set

$$P(n,L) = \prod_{j=1}^{n} \tilde{P}(j,L), \quad P(0,L) = 1$$

and obtain

$$W = \sum_{0}^{\infty} P(n,L)r^{-n}A_0 \tag{3.4}$$

and

$$W_r = -\sum_{0}^{\infty} P(n,L)nr^{-n-1}A_0$$

which we invert to find

$$A_0 = -(\sum_{1}^{\infty} nP(n,L)r^{-n-1})^{-1}W_r$$

and thus

$$(3.5)\quad W_{rr} = -\Big(\sum_{1}^{\infty} n(n+1)P(n,L)r^{-n-2}\Big)\Big(\sum_{1}^{\infty} nP(n,L)r^{-n-1}\Big)^{-1}W_r.$$

The boundary condition on W is then found by substituting in the differential equation (3.2)

$$(3.6)\quad 2iW_r = -\frac{1}{r^2}LW + \frac{1}{r}\Big[2P(1,L) + \sum_{n=2}^{\infty} n(n+1)P(n,L)r^{-n+1}\Big] \cdot \Big[P(1,L) + \sum_{n=2}^{\infty} nP(n,L)r^{-n+1}\Big]^{-1}W_r$$

and solving for W_r as a function of LW.

We simply expand the formula in powers of r but it may be better to use the approach of Enquist and Majda [5] and use other representations of the operators. What is needed is a good representation of $\sum_{n=2}^{\infty} nP(n,L)r^{-n+1}$. The first approximation is $W_r = 0$ and from (3.6) the next approximation is

$$(3.7)\qquad (2i - \frac{2}{r})W_r = -\frac{LW}{r^2} + O(r^{-4}).$$

Note that as $\omega \to \infty$, $LW \to \infty$ in general and there are problems of convergence.

In transforming to the Cauchy problem the derivative $W_r \to \tilde{W}_r + \tilde{W}_t$ and the right hand side is unchanged. Thus the radiation condition which we used was

$$(3.8)\qquad \tilde{W}_r + \tilde{W}_t = \frac{L\tilde{W}}{2\omega r^2(i - \frac{1}{\omega r})}$$

where, for the two-dimensional problem $L = \frac{\partial^2}{\partial\theta^2} + 1/4$.

To obtain the far field, that is the scattering cross section A_0, we invert (3.4) and obtain

$$A_0 = [1 - \frac{P(1,L)}{\omega r}]W \tag{3.9}$$

which is accurate to $0(\frac{1}{\omega^2 r^2})$.

4. The Difference Scheme.

To solve the time-dependent differential equation (2.7) imposing the far field condition (3.9) we have used a standard backward difference scheme for the initial value problem of a second order hyperbolic equation with second order accuracy. Let the solution to the difference scheme be $\tilde{W}(j,m,n)$ where (j,m,n) are evaluated on a grid

$$r = j\Delta r + r_0, \quad \theta = m\Delta\theta, \quad t = n\Delta t, \tag{4.1}$$

with

$$0 \le j \le N, \quad 0 \le m \le M$$

Then for an interior point,

$$(4.2) \qquad W(j,m,n+1) = T(j\pm1,j,m\pm1,m,n,n-1)$$

is determined from the values of W at $(j\pm1,m\pm1,n)$, (j,m,n), $(j,m,n-1)$. On the outer boundary $r = N\Delta r + r_0$ we use the differenced form of (3.9)

$$(4.3) \quad \frac{1}{2\Delta t}\{\tilde{W}(N,m,n+1)-\tilde{W}(N,m,n-1)\} + \frac{1}{2\Delta r}\{\tilde{W}(N+1,m,n)-\tilde{W}(N-1,m,n)\} = S(N,m,n)$$

where $S(N,m,n)$ denotes the difference approximation for the right hand side, centered differences being used in L. The value of W at $j = N+1$, m,n has to be eliminated by using the difference equation (4.2) and thus one obtains

$$(4.4) \qquad \tilde{W}(N,m,n+1) = B(N,m,m\pm1,n,n-1).$$

It still remains to apply the Dirichlet condition if there is a disturbing object or to deal with the singularity at the origin which is artificially created by the use of polar coordinates.

(a) To apply the Dirichlet condition (u=0) we simply use the given values from $\tilde{W} = -\sqrt{r}\ \exp[i\omega(x-t)]$ at the mesh point $j = 0$ for a circle or at any other boundary point. To simplify the computation we have used only boundaries consisting of sections θ = constant or r = constant.

(b) To deal with the origin we note two difficulties. First the Courant-Friedrichs-Lewy condition limits the smallest radius, i.e., we must have $r\Delta\theta > \Delta t$ for all points in the computation. Secondly, there is a singularity from the term $\frac{1}{4} r^{-2}\tilde{W}$. However, we do have $\tilde{W} \sim \sqrt{r}$. Our approach is to keep doubling the mesh size $\Delta\theta$ as $r \to 0$. Thus in these problems for $r \le r_0$ we use the mesh

(4.5) $\qquad r = j'\Delta r,\ \theta = ms(j'),\ t = n\Delta t$

where $s(j')$ is chosen so that $r\Delta\theta = j'\Delta r s(j') > \Delta t$ and so that for each j' where the mesh size $s(j')$ changes the θ-mesh is half as dense as before. The behavior of the equation at the origin itself has to be taken into account. Various integral forms of the equation could be used but it is sufficiently effective to use the equation for $\tilde{U}$ at $r = 0$ using for $\Delta\tilde{U}$ the values of $\Phi = \tilde{W}/\sqrt{r}$ at $\theta = 0, \pm\pi/2, \pi$ and $r = 2\Delta r$. By the standard difference formula along with $\Phi(n)$ for the value of $\ddot{U}$ at $r = 0$ and time $t = n\Delta t$. This yields, for the symmetric case,

$$(\Phi(n+1)-2\Phi(n)+\Phi(n-1))/(\Delta t)^2$$
$$= (\tilde{W}(2,m_1,n)+2\tilde{W}(2,m_2,n)+\tilde{W}(2,m_3,n)-4\Phi(n))/(2\Delta r)^{3/2}$$
$$+ \omega^2 n(0)\Phi(n) + \omega^2(n(0)-1)e^{-i\omega n\Delta t}.$$

Here m_1, m_2, m_3 correspond to $\theta = 0, \frac{\pi}{2}, \pi$. Note $n(0)$ means the value of the index of refraction at the origin. In the non-symmetric case there is a similar formula.

Finally we obtain $\tilde{W}(1,m,n+1)$ by interpolating the values of $\phi^{(n+1)}$ and $\tilde{W}(2,m,n+1)/\sqrt{2\Delta r}$ to obtain $\tilde{W}(1,m,n+1)/\sqrt{\Delta r}$. The error is $O(\Delta r^2)$ but turns out to be larger than in the rest of the computation.

In closing this section we shall describe our numerical method for determining when $\tilde{W}$ has reached its time harmonic steady state. Recall that the scattered field, u_s, is given by

$$u_s = [\tilde{W}e^{i\omega t}]/\sqrt{r}.$$

The bracketted term must approach $We^{i\omega r}$ as $t \to \infty$. Thus for large time $|\tilde{W}|$ becomes independent of t. We terminate our computations when

$$(4.6) \qquad \max_{\substack{0\le i\le N \\ 0\le j\le M}} \left| |\tilde{W}(n+1,i,j)| - |\tilde{W}(n,i,j)| \right| < \varepsilon$$

for some prescribed $\varepsilon > 0$.

5. Results for Model Problems.

(i) The metal cylinder.

This is a benchmark problem to test the method. Solutions have been determined by separation of variables, integral equations, and by geometrical optics [see reference 1 for a fairly comprehensive bibliography]. In [1] the "scaled cross section" $\sqrt{\frac{\pi\omega}{2}}\, S(\theta)$ is presented graphically for various frequencies. Here $S(\theta)$ is the amplitude of the outgoing cylindrical wave and θ is the polar angle with $\theta = \pi$ the direction of the incident

plane wave. These results were carefully converted to tabular form for the case $\omega a = 5$. They are shown in column C of Table 1 while the results of our present calculation are listed in column B. The areement is excellent. The relevant parameters used in the computation are $\omega a = 5$, $\Delta r = 0.1$, $\Delta\theta = \pi/40$, $\Delta t = 0.05$, and $\varepsilon = 0.01$.

For the sake of comparison the results of [2] are listed in column A. The gain over our old method is in the running time which is now approximately 1 minute on the CDC 6600. The old calculations took roughly 15 minutes on the same machine. Both methods used the same amount of core, 138K.

The effect of applying the modified radiation condition (3.9) at various distances to gain in mesh refinement was done by increasing the radius of the cylinder and applying (3.9) at a fixed radius. The relevant parameter is ωa where a is the radius of the object [see Table 1,columns D-F]. This does not, of course, refine the θ mesh.

Since our numerical method gives the total field at each grid point, the cross sections given in Table 1 represent a small fraction of the generated information. Instead of just listing these numbers an alternate method was devised to visually convey the results. First, the polar output was converted into a rectangular grid of numbers using straightforward interpolation. (This unfortunately introduces errors which tend to smear out the optical features that will be described shortly.) Then seven weights of shade were used with the darkest color corresponding

to the smallest total field while the lightest gives the largest field. The amplitude ranges are (0,2),(2,6),(6,8),(8,10),(10,14), (14,17), and (17,∞). This process gives the interference pattern shown in Figure 1 when $\omega a = 10$. The light regions correspond to constructive interference, the dark ones to destructive. Since the incident wave enters from $x = -\infty$ ($\theta = \pi$ or from the left of the figure), the total field is symmetric about the x axis and only half the pattern is shown in Figure 1. The dark semicircle is the metal cylinder. The wave patterns are readily seen in this picture. Moreover, the shadow cast by the cylinder is quite apparent. The width of the transition region which connects the deep shadow and the illuminated portions of the plane is exagerated by the interpolation process mentioned above.

(ii) Infinite Strip. (Dirichlet Case)

The diffraction by an infinite strip of half-width 2, $\{x = 0, |y| \leq 2\}$ was computed at the frequency 5, $\omega a = 10$ at the angles of attack $\alpha = 90°$ (head-on), 45°, and 90° (on edge). Here α is the angle between the incident plane wave and the positive x axis. The wave again is approaching from $\theta = \pi$. The mesh size is $\pi/20$ in θ and 0.1 in r. A variable mesh was used near the origin.

Since the interference pattern in the x - y coordinates is smeared by interpolation in this and in other cases with sharp boundaries, it is omitted here. However, the results for $\alpha = 0$ are presented in polar form in Figure 2. The numbers printed at the mesh points are ten times the total field. Thus the dark

regions now correspond to constructive interference, the light to destructive. In this picture one sees the shadow at 0, 2π, the standing wave in the illuminated region along $\theta = \pi$, the singular corners at $\theta = \frac{\pi}{2}, \frac{3\pi}{2}$ and the shadow boundaries on $y = \pm 2 = r \sin \theta$.

For the sake of brevity, we have not included the polar output for the cases $\alpha = 45°$ and 90°. Rather a few words describing these results will be offered instead. A turn through $45°(=\alpha)$ destroys the symmetry and slightly distrots the waves in the illuminated region. The shadow is shifted 45°. When the wave attacks the strip on edge ($\alpha = 90°$) there is no shadow. However, in the forward scattered direction the total field is cut in half as it should be; see [6]. The field is again symmetric.

The cross sections are presented in Table 2. They check well at 45° and qualitatively at 0° with those given in [1]. The deviation between our results and those given by [1] is probably due to the fact that the derivatives of the field become singular at the strip's edges. The coarseness of our mesh masks this problem.

The running time and core requirement for this problem were roughly the same as those needed for the metal cylinder problem.

(iii) The Helmholtz Resonator

A cylindrical Helmholtz resonator was placed in a plane wave at different angles of attack. The resonator is an infinitely thin cylinder of radius two with a strip aperture centered on the negative x axis. The angle β which subtends the aperture was taken

at different sizes. When $\beta = 0$ the resonator is a metal cylinder which was used for comparison. (The frequency was fixed at five.) The cross sections are shown in Table 3 where α is again the angle between the incident plane wave and the positive x axis. The other relevant parameters are $\Delta t = 0.05$, $\Delta r = 0.1$, and $\Delta\theta = \pi/20$. There is no data for comparison. In iterating on the closed resonator the method generated some eigenmodes in the interior. These exist as slowly damped modes as the aperture opens.

At an angle of attack of $\alpha = 0°$ and an aperture of 36° the exterior field is very similar to that generated by a metal cylinder. The interior field contains a considerable amount of energy. The amplitudes focus on the axis in two places. The strongest (maximum amplitude 5) at $x = -.5$ is a portion of caustic caused by the second reflections off the interior. The weaker focus (maximum amplitude 3) at $x = +.5$ probably corresponds to the peak of a nephroid-like caustic formed by the first reflections. The difference in strength is probably due to constructive interference.

When the wave strikes the resonator from directly behind (angle of attack = 180°) it acts like a metal cylinder. The only energy inside is diffractive and weak.

At an aperture of 180° and an angle of attack of 0° there should be a nephroid-like caustic but the edge diffraction obliterates this feature. There is marked focusing as expected, for $-2 \leq x \leq -1$. The shadow is not so sharp as with a metal cylinder. The aperture edges act like slits and smear the geometrical effects.

The core requirements for these problems were the same

as those needed for the various metal cylinders. However, the running time depends upon the aperture size which determines the complex eigenfrequencies of the resonator. Several eigenfrequencies for various resonators are computed numerically and presented in [7]. For an aperture of 36° and 800 iterations we could satisfy (4.6) only for $\varepsilon \geq .1$. However, when the aperture was 180° we could satisfy (4.6) with $\varepsilon = .05$ at 400 iterations. These two numerical examples show how the iteration scheme depends upon the eigenfrequency with the smallest imaginary part. In the first case the imaginary part is roughly 0.015 while in the second case it is about .3. If we assume that the transients decay like Exp(-.015t) in the first situation, then $t \sim 200$ would make this factor $O(1/100)$. Thus for $\Delta t = .05$ (the number used in our program) we would need in the neighborhood of 5000 iterations to obtain convergence. The same crude argument shows that about 310 iterations are needed when the aperture is 180°.

All of these problems could be solved with the addition of a variable index of refraction depending on all variables including the amplitude of the total field provided the focusing effects are weak.

(iv) Lens with variable index of refraction.

For a lens of constant index of refraction less than 1 we used (2.6), i.e. (2.8) with $n_1 = 1$, $n_2 = n$. There are no particular difficulties and the fields are qualitatively

correct. The basic lens was of radius $a \leq 3$ and the frequency $\omega \leq 5$ so that the relevant parameter $\omega a \leq 15$. For constant n less than 1 in the lens there is rapid convergence and typical lens patterns emerge. In Figure 3 the interference pattern (in the x-y plane) is shown for a lens with $a = 2$, $\omega = 5$, and $n = 0.4$. For $1 \leq n \leq 2$ there are focusing effects; e.g. when $n = 2$ the maximum amplitude is 2.8 and occurs on the axis $\theta = 0$. The full limiting amplitude principle with $n_1 = n$ and $n_2 = 1$ works well for these cases. However, $n_1 = n$ cannot be taken too large. A rescaling of time in (2.8) would introduce a large effective frequency into the exponential term. This would generate a large truncation error for a fixed Δt and cause numerical instabilities. Numerical experiments confirmed this observation for $n_1 = n \geq 8$ and $\Delta t = .05$. On the other hand, taking $n_1 = 1$, $n_2 = n$ brings immediate instability into the computation.

More interesting effects occur if $n = n(r)$ or $n = n(r,\theta)$. For example, geometrical optics predicts [see reference 8] that for $n = r^2/9$, $r \leq 3$, $n = 1$, $r \geq 3$ that there will be focusing at $(3,\frac{\pi}{2})$. At $\omega = 5$ we obtained an amplification of 2.5 in the total field at that point. Also there is a geometrical shadow on $\theta = \frac{\pi}{2}$. This shadow (for a finite ω) is not sharp because a single ray on $\theta = 0$, $\theta = \pi$ passes through it.

A second case, a Luneberg lens with $n = 2 - r^2/9$ for $r \leq 3$, $n = 1$ for $r \geq 3$ focused at $(3,0)$ with a magnitude of 3. This point is a focus for the geometrical optics rays.

The general case $n = n(r,\theta)$ was tried with $n = (r^2 - r_0^2)/(9 - r_0^2)$ for $r \leq 3$, $n = 1$ for $r \geq 3$, where $r_0 = 2 - 0.5 \cos^2(\theta/2)$. The

particular effects are not of interest. Obviously the oscillations in n cannot be too large without destroying accuracy. What is important is that this problem cannot be solved by separation of variables. Geometrical optics is complicated and an integral method would involve inverting a kernel in four variables. No difficulties are encountered here. There is some increase in memory since n depends on two variables. The running time was again about a minute. Condition (4.6) was satisfied for $\epsilon = .01$ with $\omega = 5$, $a = 3$.

(v) A Model of an Overdense Plasma.

An overdense plasma column can be modelled by an index of refraction which becomes negative, such as the example used, $n = (r^2-4)/5$ for $r \leq 3$, $n = 1$ for $r \geq 3$. Geometrical optics predicts [9] a caustic on the ellipse $\frac{x^2}{4} + \frac{y^2}{9} = 1$.

Figure 4 shows the calculated field in polar coordinates with $\omega = 5$, $a = 2$, $\Delta t = 0.05$, $\Delta r = 0.1$, and $\Delta\theta = \pi/40$. Recalling that the larger (hence darker) numbers correspond to constructive interference note that the ellipse (heavy curve) lies very close to the edge of the constructive interference for $\pi/2 \leq \theta \leq \pi$. The rest of the shadow is cast by the caustic along the line $y = r\sin\theta = 3$ (remaining portion of the heavy curve for $r \geq 3$, $\theta \leq \pi/2$). Figure 5 shows the x-y plot of the interference pattern where the lighter regions now correspond to constructive interference. The amplitude ranges for the various shades are again (0.2), (2,6),(6,8),(8,10), (10,14),(14,17), and (17,∞). Unfortunately the interpolation required for the rectangular output smears out the caustic.

6. Conclusions.

There are four obvious dimensionless parameters in the computed problem, $\omega\Delta r$, $\omega r\Delta\theta$, ωa and ωr_0 where a is a relevant length and r_0 is the value of r where the radiation condition is imposed. The square of the first two enter the errors produced by the second order difference scheme and in most of our calculations was approximately .2. The third measures the relevance of geometrical optics and ranged up to 15. The last one, usually about .025, arises from an expansion at ∞ for fixed ω. The error terms are of order $(\omega r_0)^{-3}$ but the coefficients are singular as $\omega \to \infty$.

In many of the problems there were discontinuities, infinitely thin objects or discontinuities in the index of refraction. These induce discontinuities in the second derivatives of the time dependent solution and in the steady state. In spite of this source of inaccuracy there was remarkable agreement with known results and there is probably some cancellation of error.

The method could be applied to higher dimensional phenomena where the reflecting object as well as variable index of refraction are not amenable to solution by integral equations. Since the problem is solved by a very straight forward difference scheme it should be easily effected by vector computation. Other problems where variations of the limiting amplitude principle could be used involve Maxwell's equations, and wave propagation in water.

Finally, the method has been modified slightly and applied to the interesting and important case of a nonlinear medium [12]. In that report

$$n = n_0 + \gamma(1 - n_0)|U|^2$$

where n_0 is the index of refraction used in our overdense plasma model and γ is a constant which controls the strength of the nonlinearity. The results were excellent; the effects of refraction and self-focusing could be discerned and controlled by varying γ. In particular, self-focusing amplifies the fields near the origin as was first observed by F. Tappert [unpublished results].

BIBLIOGRAPHY

(1) J.J. Bowman, T.B.A. Senior, and P.L.E. Uslenghi, Electromagnetic and Acoustic Scattering by Simple Shapes, North-Holland, Amsterdam, 1969.

(2) G.A. Kriegsmann and C.S. Morawetz, Numerical Solutions of Exterior Problems with the Reduced Wave Equation, Journal of Computational Physics, 28(1978), pp. 181-197.

(3) A. Bayliss and E. Turkel, Boundary Conditions for Exterior Acoustic Problems, Report No. 79-7, ICASE, NASA Langley Research Center, 1979.

(4) J. Weidmann, A Virial Theorem and its Application to the Spectral Theory of Schrödinger Operators, Bulletin of the American Mathematical Society, 73(1967), pp. 452-456.

(5) B. Engquist and A. Majda, Absorbing Boundary Conditions for the Numerical Simulation of Waves, Mathematics of Computation, 31(1977), pp. 629-652.

(6) R.N. Buchal and J.B. Keller, Boundary Layer Problems in Diffraction Theory, Communications in Pure and Applied Mathematics, 13(1960), pp. 104-105.

(7) T.B.A. Senior, Electromagnetic Penetration into Cavities. IEEE Journal on Electromagnetic Compatability, 18(1976), pp. 71-73.

(8) N.G. Alexopoulos, On the Refractive Properties of Media with Poles or Zeroes in the Index of Refraction, IEEE Transactions on Antennas and Propagation, 22(1974), pp. 242-251.

(9) G.A. Kriegsmann, An Application of the Method of Geometrical Optics to the Scattering of Plane Electromagnetic Waves off Cylindrically Confined Cold Plasmas, Journal of Mathematical Physics, 17(1976), pp. 112-120.

(10) C.S. Morawetz, The Limiting Amplitude Principle, Comm. Pure Appl. Math., Vol. XV, 3. 1962, pp. 349-362.

(11) H.O. Kreiss, Initial Boundary Value Problems for Hyperbolic Systems, Comm. Pure Appl. Math., Vol. XXIII, 1970, pp. 277-298.

(12) G.A. Kriegsmann and C.S. Morawetz, Computations with the Non-linear Helmholtz Equation, submitted to the Journal of Applied Optics.

Figure Captions

Figure 1: The interference pattern produced by the total field's amplitude, $|U|$, for a metal cylinder. The light regions correspond to constructive interference, the dark to destructive. The dark semicircle is the cylinder. The relevant parameters are $\omega a = 10$, $\Delta r = 0.1$, $\Delta\theta = \pi/40$, and $\Delta t = 0.05$.

Figure 2: The total field's amplitude, $|U|$, in polar coordinates for a metal strip with the incident wave normalized to 10. The incident wave strikes the strip head on ($\alpha = 0$). The set of points $\{(r,\theta)|\theta = \pi/2, 3\pi/2, 0 \leq r \leq 2\}$ represents the strip in polar coordinates. Since the numbers printed are the actual field values, the dark regions now correspond to constructive interference, the light to destructive. The relevant parameters are the same as in Figure 1 except $\Delta\theta = \pi/20$.

Figure 3: The interference pattern produced by the total field's amplitude, $|U|$, for a dielectric lens with $n = 0.4$ The relevant parameters are $\omega a = 15$, $\Delta r = 0.1$, $\Delta\theta = \pi/20$, and $\Delta t = 0.05$.

Figure 4: The total field's amplitude, $|U|$, in polar coordinates for an overdense plasma column. The incident wave was normalized to 10. The heavy curve represents the caustic $\frac{x^2}{4} + \frac{y^2}{9} = 1$, when $r \leq 3$ and the geometric shadow $y = 3$ when $r \geq 3$. The relevant parameters are $\omega a = 15$, $\Delta r = 0.1$, $\Delta\theta = \pi/40$, and $\Delta t = 0.05$.

Figure 5: Same physical problem and relevant parameters as Figure 4. However, this is now the interference pattern in x-y coordinates with the light regions corresponding to constructive interference, the dark to destructive.

Legend for Table 1: Columns A-F present the cross section $(\frac{\pi\omega}{2})^{1/2} S(\theta)$, for a metal cylinder with $u_s \sim S(\theta)\frac{e^{i\omega r}}{\sqrt{r}}$, $\Delta t = 0.05$, and $\Delta\theta = \pi/40$.

Column A contains the results given in [2], B presents a tabulated version of the data given graphically in [1], and columns C-F contain the results of our new calculations.

Legend for Table 2: Columns A-D present the cross section $(\frac{\pi\omega}{2})^{1/2} S(\theta)$, for a metal strip with $u_s \sim S(\theta)\frac{e^{i\omega r}}{\sqrt{r}}$, $\Delta t = 0.05$, $\Delta r = 0.1$, and $\Delta\theta = \pi/20$.

Columns A and D present tabulated versions of data given graphically in [1]. Columns B and C contain the results of our new calculations. The parameter α is the angle between the incident plane wave and the normal to the strip. L is the length of the strip.

Legend for Table 3: Columns A-C present the cross section $(\frac{\pi\omega}{2})^{1/2} S(\theta)$, for various Helmholtz resonators with $u_s \sim S(\theta)\frac{e^{i\omega r}}{\sqrt{r}}$, $\Delta t = 0.05$, $\Delta\theta = \pi/20$, and $\Delta r = 0.1$. The parameter α is the angle between the incident plane wave and the positive x axis while β is the aperture angle of the resonator. The parameter $\omega a = 10$ where a = radius of the resonator.

Table 1

θ(°)	A ωa=5	B ωa=5	C ωa=5	D ω=10,a=1	E ω=5,a=2	F ω=5,a=4
0	5.67	6.05	6.05	11.33	10.84	12.49
9	5.30	5.25	5.29	6.63	7.20	10.15
18	3.78	3.30	3.34	2.11	3.72	11.15
27	2.10	1.75	1.70	3.21	3.[illegible]	13.50
36	1.81	1.75	1.77	2.50	3.55	14.71
45	2.00	1.95	1.99	2.61	3.41	15.04
54	1.89	1.75	1.81	2.54	3.32	14.97
63	1.74	1.68	1.73	2.55	3.23	14.74
72	1.79	1.75	1.80	2.56	3.18	14.41
81	1.86	1.80	1.83	2.56	3.10	13.91
90	1.86	1.82	1.82	2.56	3.04	13.12
108	1.93	1.88	1.86	2.57	2.88	10.60
126	1.97	1.92	1.89	2.55	2.79	7.51
144	1.99	1.93	1.91	2.55	2.76	5.02
162	1.99	1.94	1.93	2.59	2.75	3.97
186	2.00	1.95	1.96	2.55	2.76	3.88

Table 2

θ(°)	A α=45°, ωℓ=10	B α=45°, ωℓ=10	C α=0°, ωℓ=10	D α=0°, ωℓ=10
-90	.89	.41	.32	.00
-81	.89	.85	.96	.00
-72	.89	.19	.09	.00
-63	.89	1.31	1.0	.83
-54	1.20	1.72	1.9	1.8
-45	.90	1.62	2.6	1.5
-36	1.20	1.60	2.8	.9
-27	1.20	1.64	3.3	2.6
-18	1.20	1.52	3.6	0.0
-9	1.50	1.49	6.2	7.0
0	1.66	1.88	8.1	9.9
9	1.80	1.71	6.2	7.0
18	2.10	2.08	3.6	0.0
27	5.96	2.40	3.3	2.6
36	7.20	5.40	2.8	.9
45	5.37	7.30	2.6	1.5
54	2.98	5.61	1.9	1.8
63	1.49	2.50	1.0	.83
72	1.05	1.30	.09	.00
81	.70	1.05	.96	.00
90		.68	.32	0.0

Table 3

	A	B	C
θ(°)	β=36°,α=0	β=36°,α=180°	β=180°,α=0°
0	8.86	2.70	8.55
9	6.81	2.71	6.83
18	4.10	2.73	4.11
27	4.11	2.75	4.01
36	3.99	2.79	3.73
45	4.06	2.85	3.39
54	4.01	2.96	2.58
63	4.01	3.11	1.38
72	3.97	3.30	.84
81	3.86	3.50	1.39
90	3.71	3.70	1.09
99	3.53	3.85	1.86
108	3.42	3.99	2.15
117	3.50	3.95	3.12
126	3.72	4.15	3.73
135	3.83	3.83	2.85
144	3.66	4.25	3.55
153	3.28	3.87	5.55
162	2.48	3.77	3.78
171	1.10	7.60	2.99
180	1.36	8.48	5.32

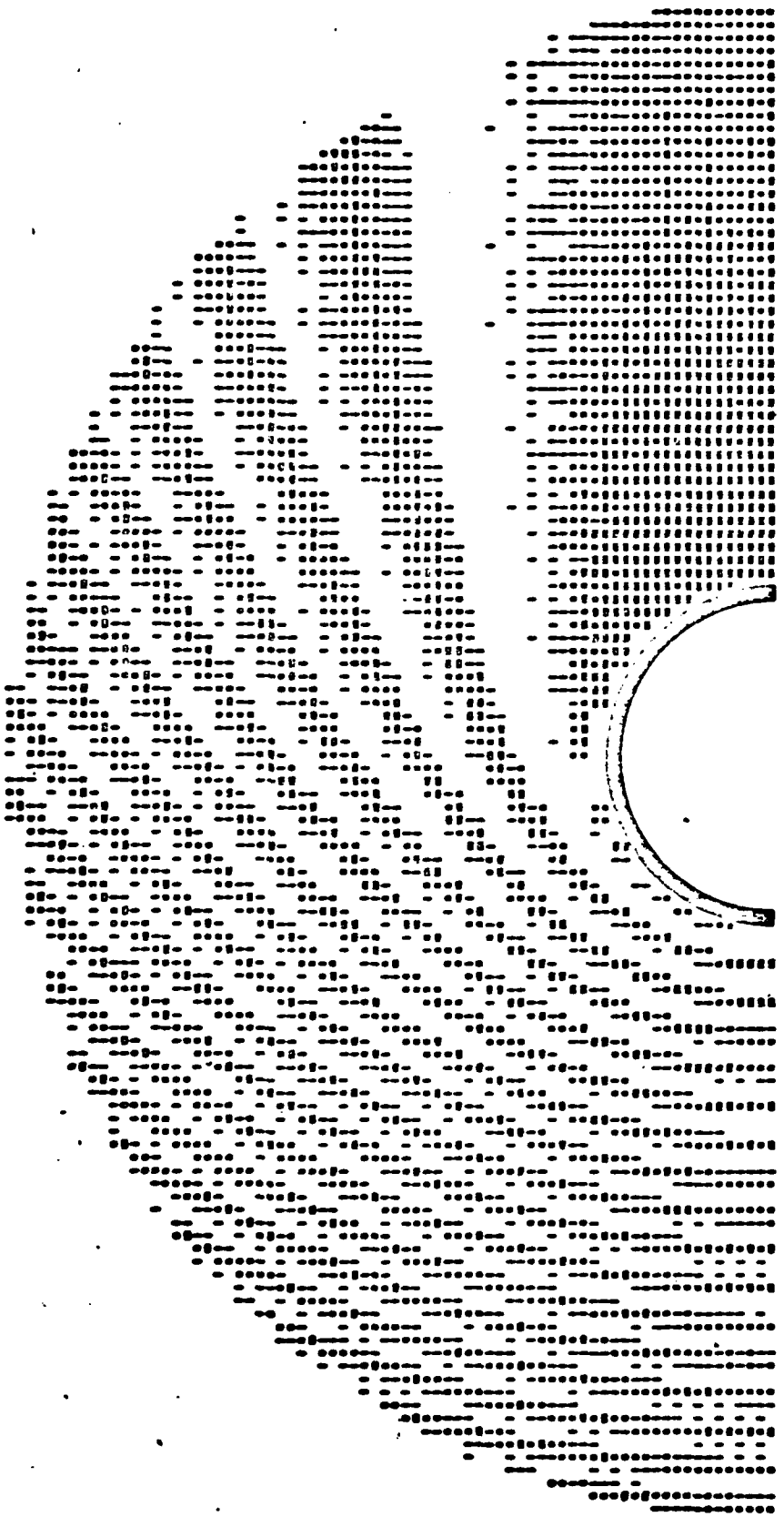

90
180
270

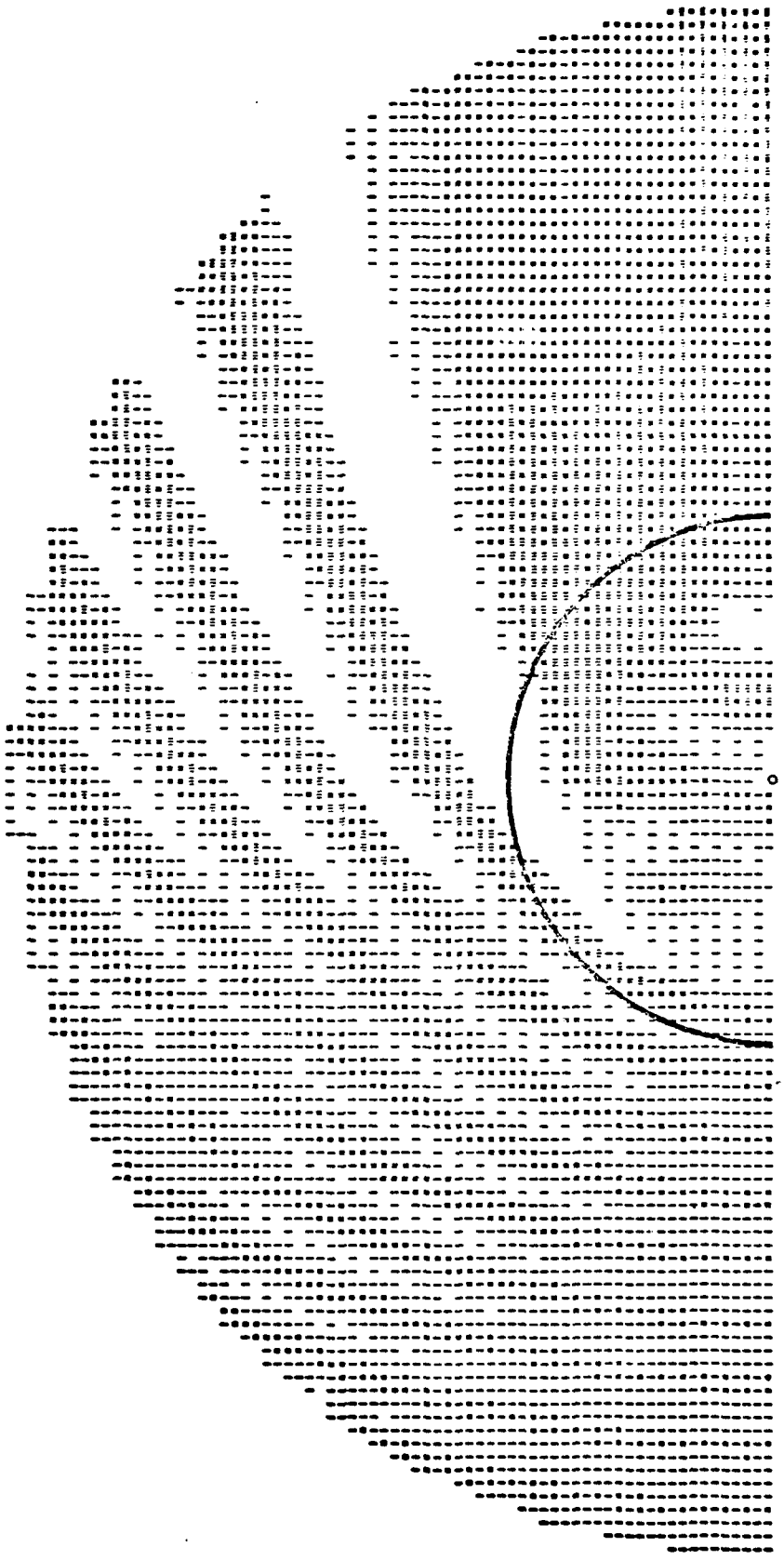

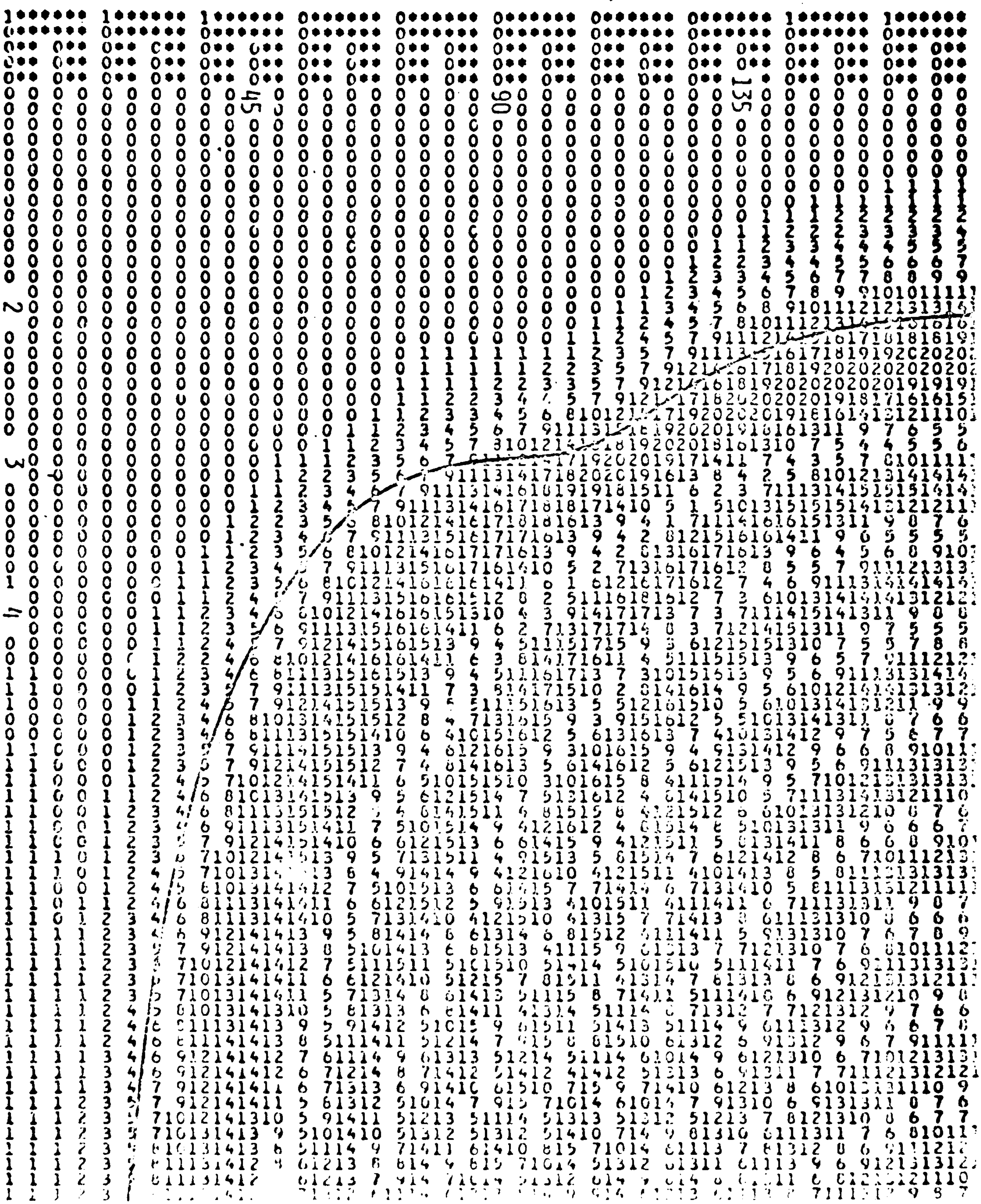
4.
45
90
135
2
3
4